

Simulation of EUV XMM MM image from actual measurements

Y. Stockman, P. Barzin, H. Hansen, J.Ph. Tock
Centre Spatial de Liège, Université de Liège
Av. du Pré-Aily, B-4031 Angleur, BELGIUM
phone : +32 43676668 ; fax : +32 43675613 ; email : ystockman@ulg.ac.be

D. de Chambure, Ph. Gondoin
ESA / ESTEC PO BOX 299, 2200 AG Noordwijk, THE NETHERLANDS
phone : +31 715656565 ; fax : +31 71 5654895

ABSTRACT

In the frame of the XMM Mirror Module (MM) optical tests at Centre Spatial de Liège (CSL), a large number of images have been recorded. Most of the images are taken at the He I line (58.4 nm), and some at He II line (30.4 nm). At this long wavelength range compared to the X-Ray, the image quality is merely affected by low frequency figuring errors of the Mirror Shell (MS). The telescope response is available for the 4 Flight Model (FM) MMs without considering any other optical subsystem i.e. the Reflecting Grating Assembly (RGA) and the X-Ray Baffle (XRB). In order to take into account the presence of straylight, images are taken at off axis angle up to several degrees. The efficiency of the XRB was demonstrated qualitatively and quantitatively. The optical performances of two out of three MMs fully assembled that will be integrated on the XMM satellite are presented. This means :

- the MM FM2 with its XRB, that will provide images directly on an European Photon Imaging Camera (EPIC)
- the MM FM3 with its XRB and FM2 RGA and exit baffle (EXB) that provides images on an EPIC and on a RGA Focal plane Camera (RFC).

The paper also summarises the way these images were taken and the information that are available from this data. To conclude a simulation of a XMM image using this experimental data is performed.

1. INTRODUCTION

In the frame of XMM Mirror Module a large number of tests have been performed to characterise and space qualify each MM. All the MMs have been submitted to at least 5 test sequences. There is a first reference test to characterise the MM after the manufacturing process¹, and a second one to space qualify the MM which consists in the verification of the optical performance integrity after vibration and thermal cycling tests. A third test sequence is devoted to acquire reference performance before the XRB (X-Ray Baffle) integration. The alignment and the efficiency of the XRB is then checked during the fourth sequence². The last test sequence is devoted to complementary tests, which can include the RGA (Reflection Grating Assembly) integration³.

During all these tests a large quantity of information has been recorded, and up to now not all of them have been fully analysed. The purpose of this paper, is neither to present the XMM MM already considered in ref 4, 5 and 6, nor to describe the Focal X facility^{7,8,9} in which the tests have been performed. The paper will mainly focus on the information acquired during all these test campaigns. It will shortly introduce the various optical channels used, and the data reduction performed. Using the on and off-axis images as well as the straylight distribution in the near Field Of View (FOV) an image is processed to give an example of an image obtained through XMM optics.

2. EUV ON AXIS IMAGES

EUV focal images are recorded with an EUV collimator. The advantage¹⁰ of this concept is to fully illuminate the MM, with a perfectly parallel beam. The use of EUV wavelength is necessary to minimise the diffraction contribution. Using shorter wavelengths was not possible with X-Ray optics state-of-the-art and the required schedule. EUV data provides the Point Spread Function (PSF) of the MMs on-axis for low and mid frequency figuring error of the MSs. The main disadvantage is to characterise the system outside its working energy range. This means that the measurements are not fully representative of the scattering effect, however this information is available from X-Ray pencil beam measurements and tests at the Max Planck Institute Panter facility. Tilt motors located under the test adaptor supporting the MM allow to measure the PSF in the complete Field Of View (FOV) (± 15 arcmin) of the MMs.

In this paragraph only the on-axis PSF images after the integration of the XRB are presented. Previous papers^{1,2} have demonstrated that the environmental tests and the XRB integration do not degrade the on-axis image quality. The pictures in figure 1 (b and c) are the actual PSF for the MMs FM1 and FM2 where no RGA is mounted. For MMs FM3 and FM4 a RGA is mounted approximately 500 mm away from the MM exit plane. Presently only the final PSF for the MM FM3 with the RGA FM2 is available. The MM FM4 with RGA FM1 combination is currently under testing. The introduction of the RGA degrades slightly the EPIC best focus image. One explanation is a diffraction contribution of the nested design of the RGA. A best focus image of the MM QM is also presented. By comparison to the FM images, there is undoubtedly a clear improvement : the main reason is the better integration (focusing and centring) of the mirror shells on the spider¹¹.

The figures hereafter present the best focus PSF in logarithmic scale of all the manufactured MMs. The table 1 provides a quantification of the figures 1 by giving the results of the computation of the Half Energy Width (HEW), 90 Energy Width (90EW) and the Full Width at Half Maximum (FWHM).

Figure 1.a : MM QM PSF

The MM QM consists in a MM with 21 optical MSs (9 large and 12 small size) and 37 optically not representative MSs. 3 D views of the PSF show that the central core consists not in a unique peak, but in two separated peaks. One comes from the small size MSs group the other one from the large size MSs group. The distorted PSF comes mainly from the distortions of the large MSs at their edge due to deformations of the spider.

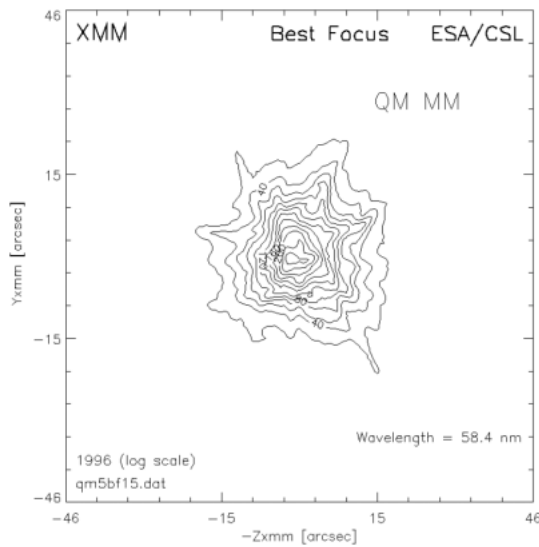


Figure 1.b : MM FM1 PSF

This first MM FM with 58 MSs shows the improvement of the mirror manufacturing and of integration processes. The central core consists in a single peak. The HEW of this image is 25 % better than the one achieved with the MM QM. Extra focal images show also nice circular shape without outgoing “loops” as it was the case with the MM QM.

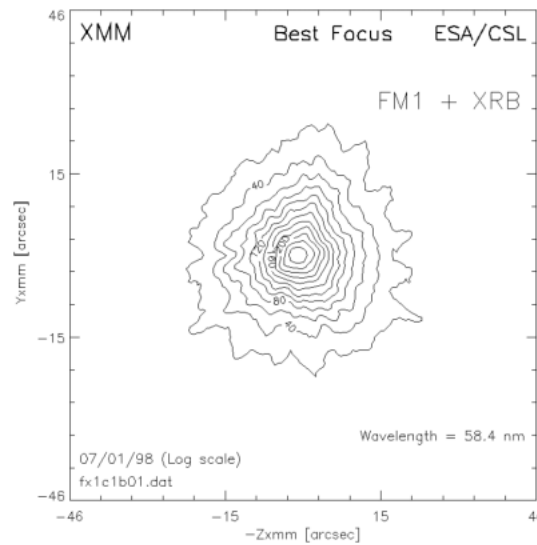


Figure 1.c : MM FM2 PSF

The MM FM2, which will be integrated on the payload in front of EPIC p-n detector, has the same resolution (HEW) as MM FM1. The major reason of the triangular shape is due to interface flatness unevenness (few μm) between the spider supporting the mirrors and the interface structure.

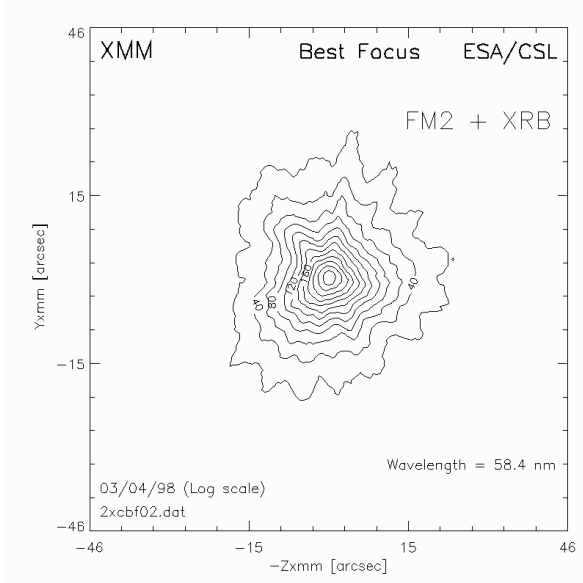


Figure 1.d : MM FM3 PSF

The MM FM3 is the one presenting the best PSF in terms of geometry and EEF in the EUV. The PSF is slightly pentagonal but present nice circular symmetry. Extra focal images show that there is almost no deformation on the large MSs due to integration. This MM will be integrated on the spacecraft with the RGA FM2.

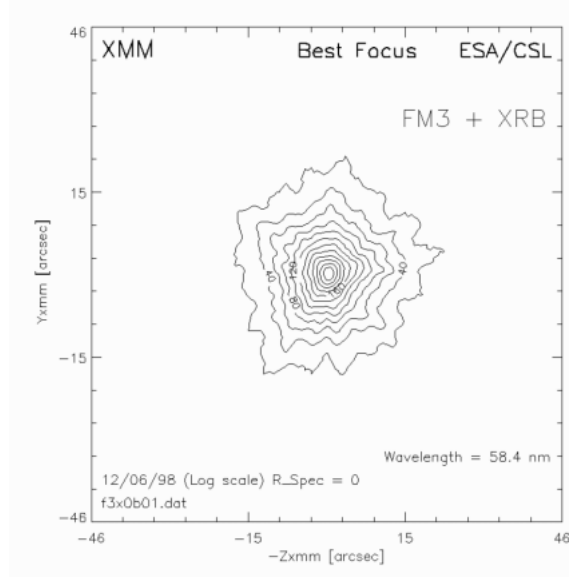


Figure 1.e : MM FM4 PSF

The MM FM4 on axis PSF, is as good as the one of the MM FM3. This MM will be integrated with RGA FM1. As for MM FM2 the triangularisation of the PSF shape is mainly due to the Mirror Interface support integration on the spider.

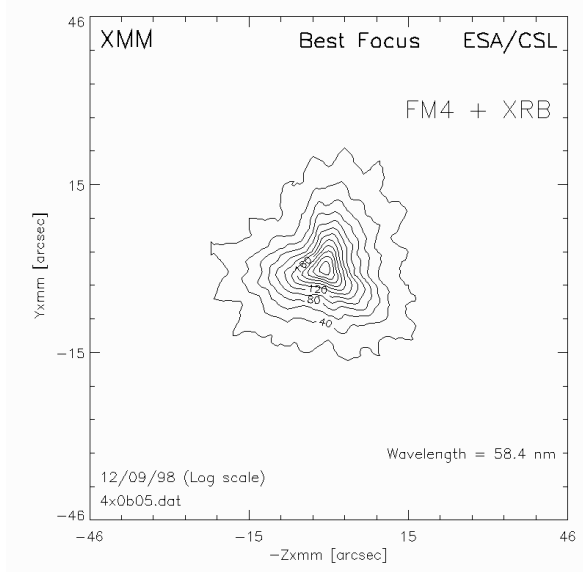


Figure 1.f : MM FM3 + RGA2 PSF

FM3 MM on axis PSF with RGA FM2 integrated. This corresponds to the EUV on axis final image for this flight configuration. During this test the exit baffle was also integrated.

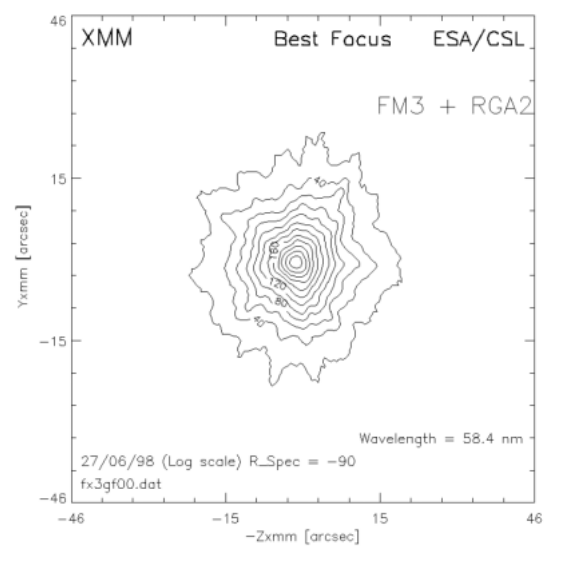


Table 1 : HEW, 90EW and FWHM computed at best focus for QM and for FM MMs

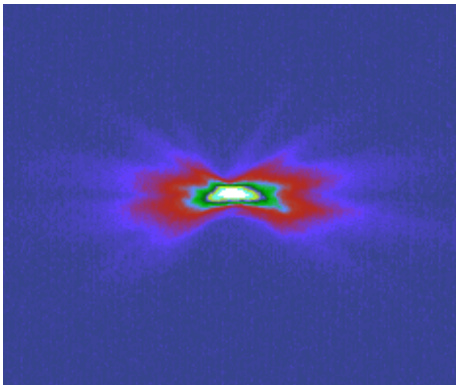
Mirror Module [arcsec]	QM	FM1	FM2	FM3	FM3 + RGA	FM4
HEW	19	15.5	15.4	14.2	15.4	14
90EW	79	62.6	62.5	61.8	63	60.7
FWHM	11	6.7	6.3	4.5	5.5	4.9

3. EUV FOV IMAGES

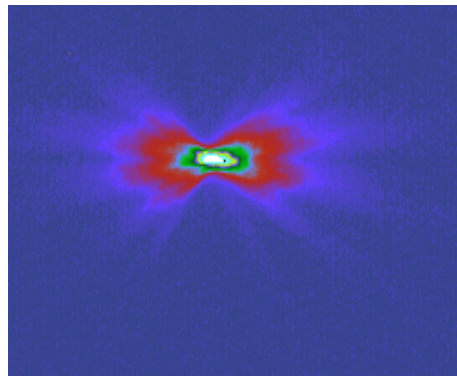
The PSF in the complete FOV has been measured following two orthogonal axes with an angular step measurement of 3.5 arcmin for the MM FM2 with XRB. This is the final optical flight configuration. Some results of these two angular scans are given in figure 2. For the MM FM3 + XRB + RGA flight configuration, the PSF in the FOV has been measured following two orthogonal axes with an angular step of 3 arcmin. The same measurements are realised on the MM FM4. The final data is not yet available. The reduction of these images in terms of HEW (figure 3), shows a HEW invariance over a FOV of +/- 6 arcmin. Field curvature measurements have also been performed on FM1 MM. The results fit with the modelled one. These tests have not been performed on FM2 and FM3 MM for planing reasons.

Figure 2 : Examples of images in the FOV at 58.4 nm of MM FM2 with XRB

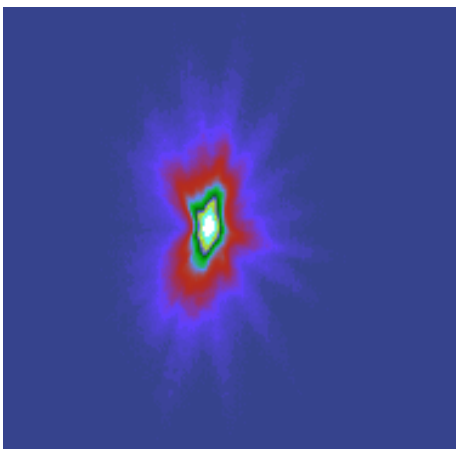
-21 arcmin around Y xmm



+21 arcmin around Y xmm



-10.5 arcmin around Z xmm



+17.5 arcmin around Z xmm

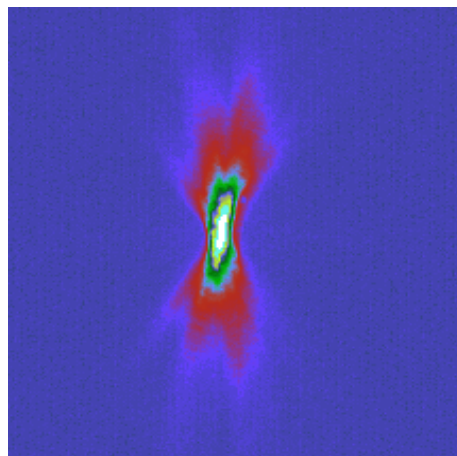
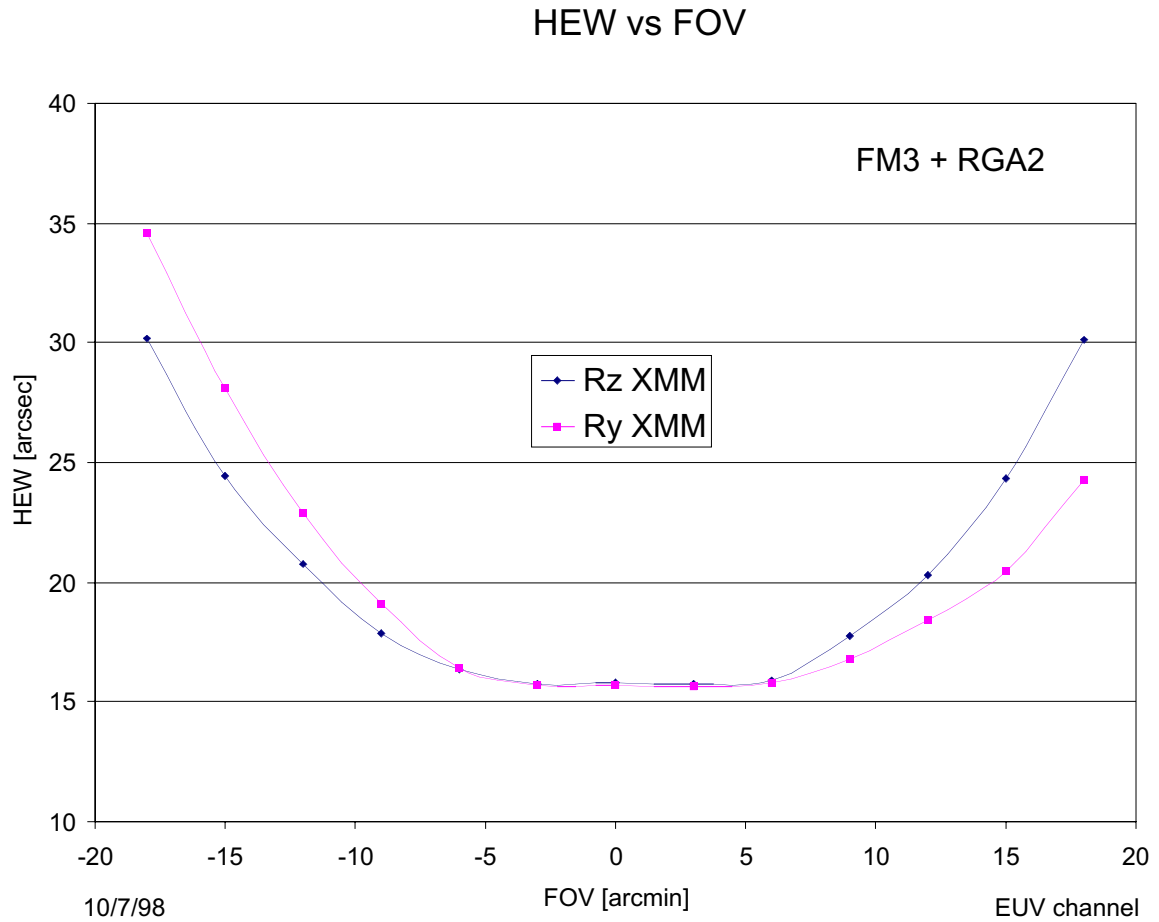


Figure 3 : HEW versus the FOV at 58.4 nm of MM FM3 with XRB and RGA2 following two orthogonal axis



4. EUV STRAYLIGHT IMAGES

The facility has been designed to allow measurements of straylight in the FOV of the EPIC and RFC detectors. This is performed by tilting the optical bench (with the telescope) with respect to the EUV collimator. In this configuration the EUV CCD detector moves with the MM as a complete telescope. By translating the EUV CCD over 9 adjacent positions, it is possible to cover the full EPIC area. The accessible angular range is -2 to $+7$ arcdegrees. The measurements have been particularly focused on the angular range between 30 and 90 arcmin, where the higher straylight level are observed (figure 4). It is also for this angular range that the XRB has been designed. Measuring straylight level before and after the XRB integration allows to evaluate the XRB efficiency as presented in figure 6. In the figures 4 the efficiency of the XRB is clearly demonstrated qualitatively for the FM4 MM. The straylight collecting area is a few square centimetres over the complete EPIC detector. This is to be compared to the 1550 cm^2 of a point source. In conclusion, the images of figure 4 will be negligible with respect to a point source. The straylight could slightly degrade the image only if a wide and intense straylight source is present in the near FOV. The introduction of the RGA modifies these straylight patterns. This one blocks the straylight, in such a way that the single hyperbola reflections are dotted as it is shown on the images of figures 5.b and d. Before and after XRB integration, the vignetting function of the MM is measured. This gives an evaluation of the attenuation of the image in the FOV due mainly to the MS and the XRB vignetting. This doesn't take into account the loss by reflectivity. Indeed the reflectivity at 58.4 nm doesn't vary a lot (less than 1%) for incident angles between 0 and 1 arcdegrees. To take into account the effect of reflectivity, X-Ray measurements have been performed with a pencil beam at various energy lines.

Figure 4 : Straylight reduction by the XRB for the MM FM4 at 30, 40, 50 and 60 arcmin

The left images are the straylight images without XRB. The observed rings come from single reflection on the hyperboloids of the mirrors. Once the XRB is integrated the number of single reflection decreases. In terms of integrated effective area over the EPIC FOV this corresponds to a reduction by a factor 5 to 10. During these tests “unexpected” rings crossing the detector from 25 to 35 arcmin FOV have been observed. This is due to back reflection on some small MSs. These non simulated straylight rings are observable due to the high sensitivity of the measurements (less than 1 cm² in terms of EUV effective area).

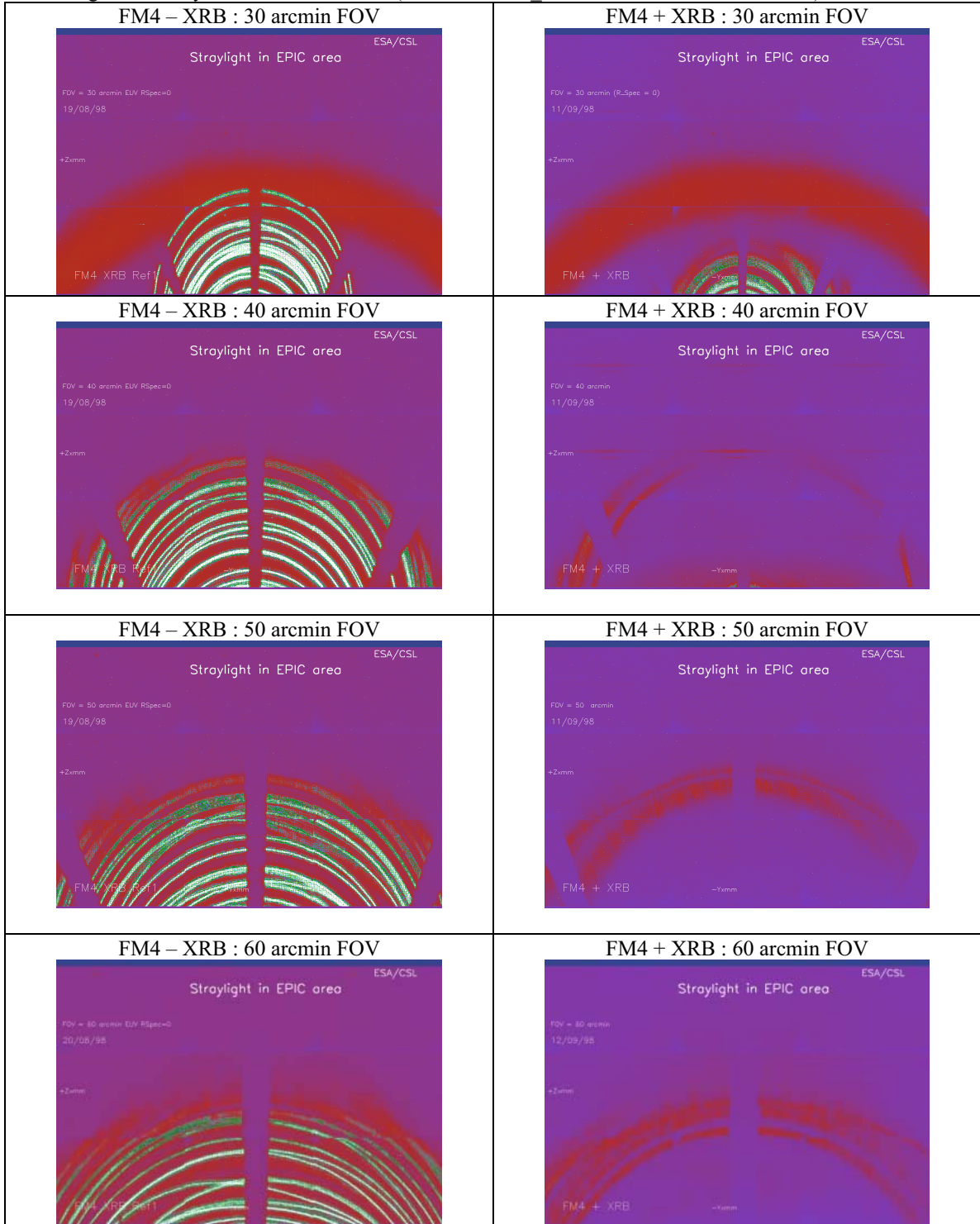


Figure 5 : Straylight behaviour on the MM FM3 with RGA

The first left image presents the straylight pattern after the XRB integration. This pattern is the same for any rotation around the XMM optical axis. Once the RGA is integrated, the axis-symmetry is lost. The 3 next pictures give the situation after the RGA integration. Two images are taken in the direction of the RGA dispersion and only one in the cross dispersion direction because of symmetry. The 4 images are acquired with off-axis field angle of 50 arcmin.

Figure 5.a : Straylight on FM3 after XRB integration and before RGA integration

The single hyperbola reflections are attenuated by the presence of the XRB.

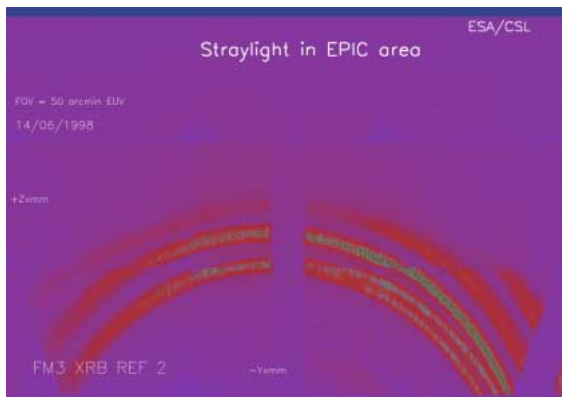


Figure 5.b : Straylight on FM3 with XRB and RGA2 integrated

The RGA integration reduces the straylight by simple vignetting. This reduction is about 50 %. The observed shadowing is due to the supporting structure (rail) of the RGA gratings.

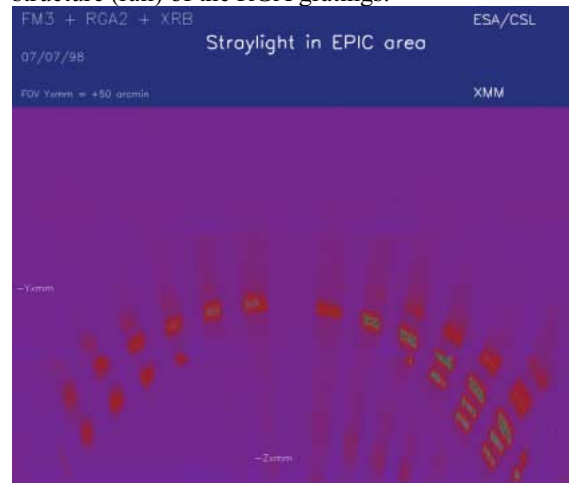


Figure 5.c : Straylight on FM3 with RGA2

For stars in the opposite direction the straylight behaviour is different due to the asymmetry introduced by the RGA.

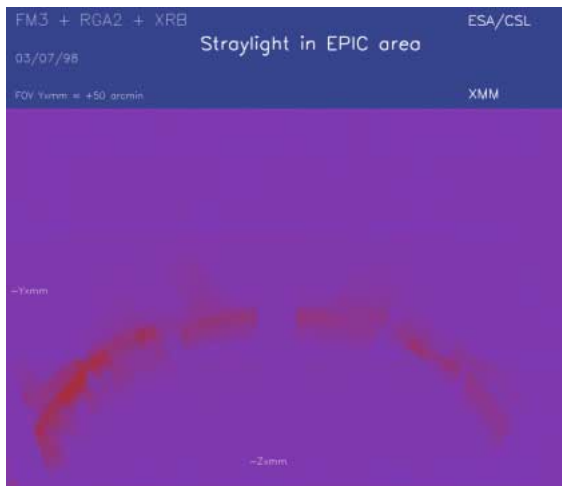


Figure 5.d : Straylight FM3 with RGA2

For rotations around the dispersion axis, the straylight figure is sign independent. Vignetting of the grating is also observed. The reduction of straylight is lower than in the other direction.

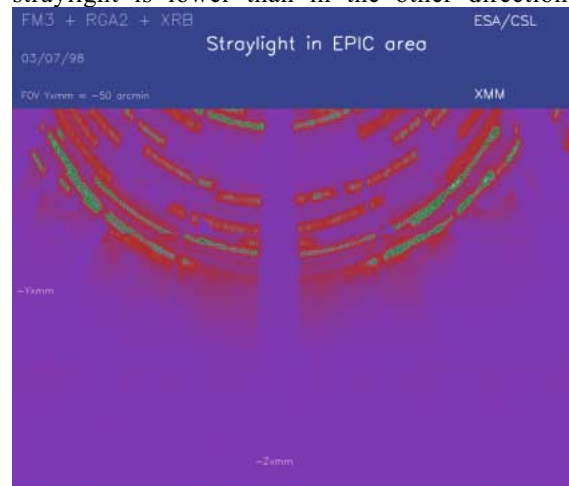
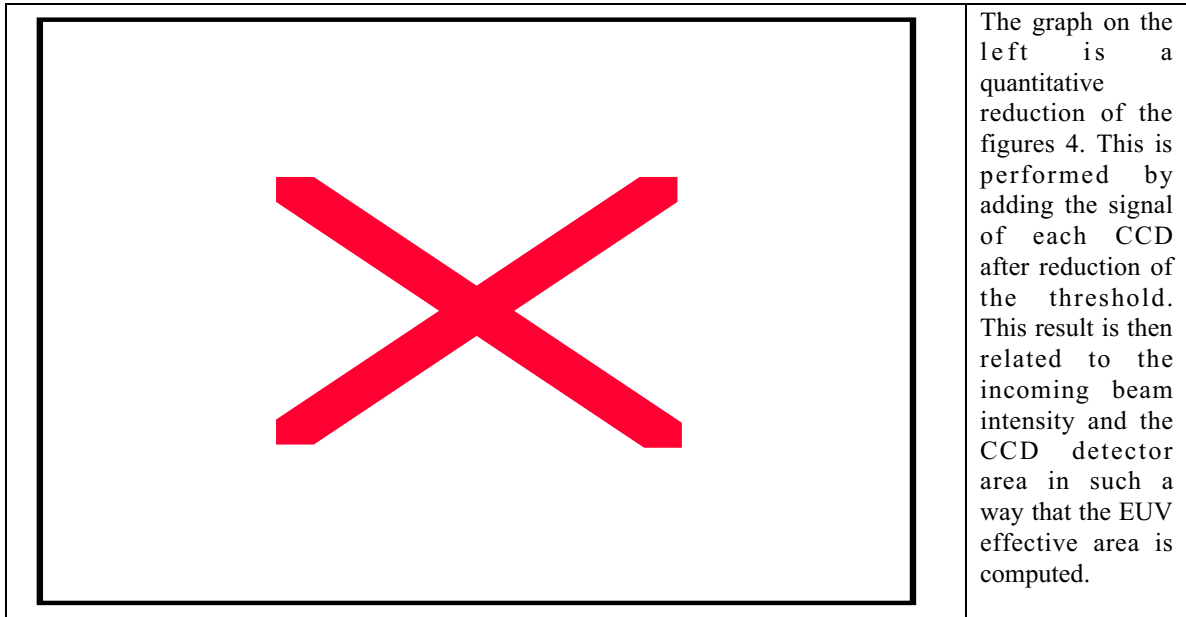


Figure 6 : EUV effective area in EPIC FOV for straylight angle up to 80 arcmin on MM FM3

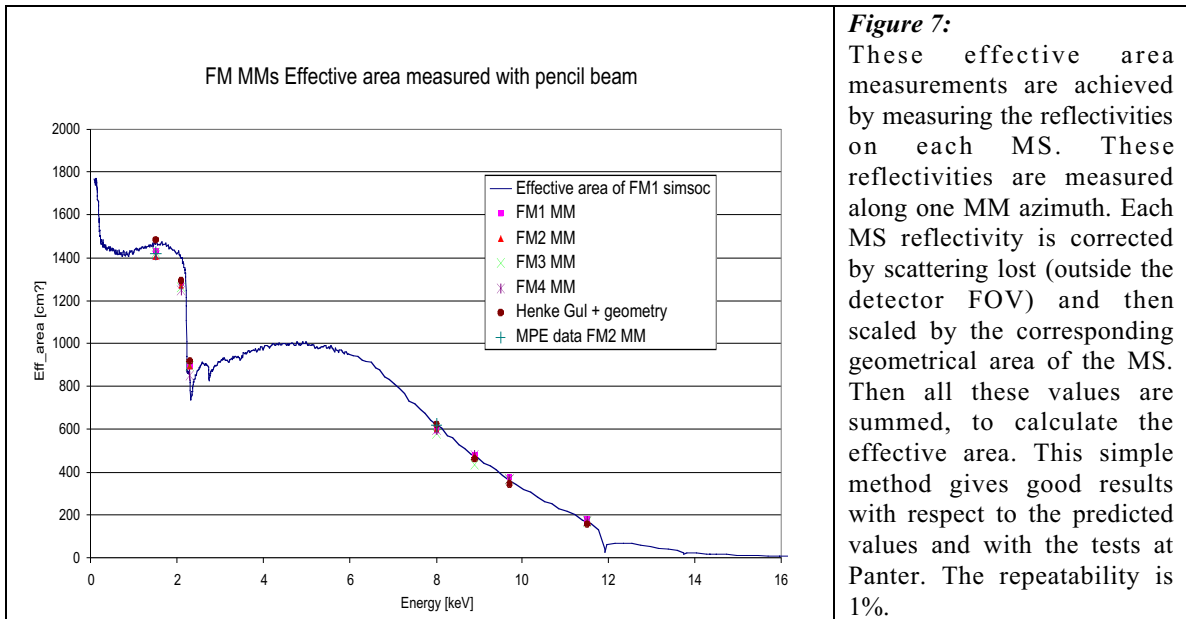


5. X-RAY MEASUREMENTS

X-Ray measurements are performed using a pencil beam. It consists in two pinholes with a diameter of 0.3 mm separated by about 7.5 m. This configuration provides a 0.5 mm diameter X-Ray pencil beam at the MS entrance plane. Therefore only local measurements are performed. The main functions are to measure the position of each MS relatively to each other, the reflectivity of the MSs and the wing scattering of the MSs. This information are useful to :

- ❖ Verify the MS positioning in between each environmental tests
- ❖ Verify the correct alignment of the XRB
- ❖ Evaluate the MM effective area
- ❖ Evaluate the wing scattering behaviour of a MS.

An example of the achieved data is presented in the figure 7. It is observed that the evaluated effective area fits fairly well the predicted values.

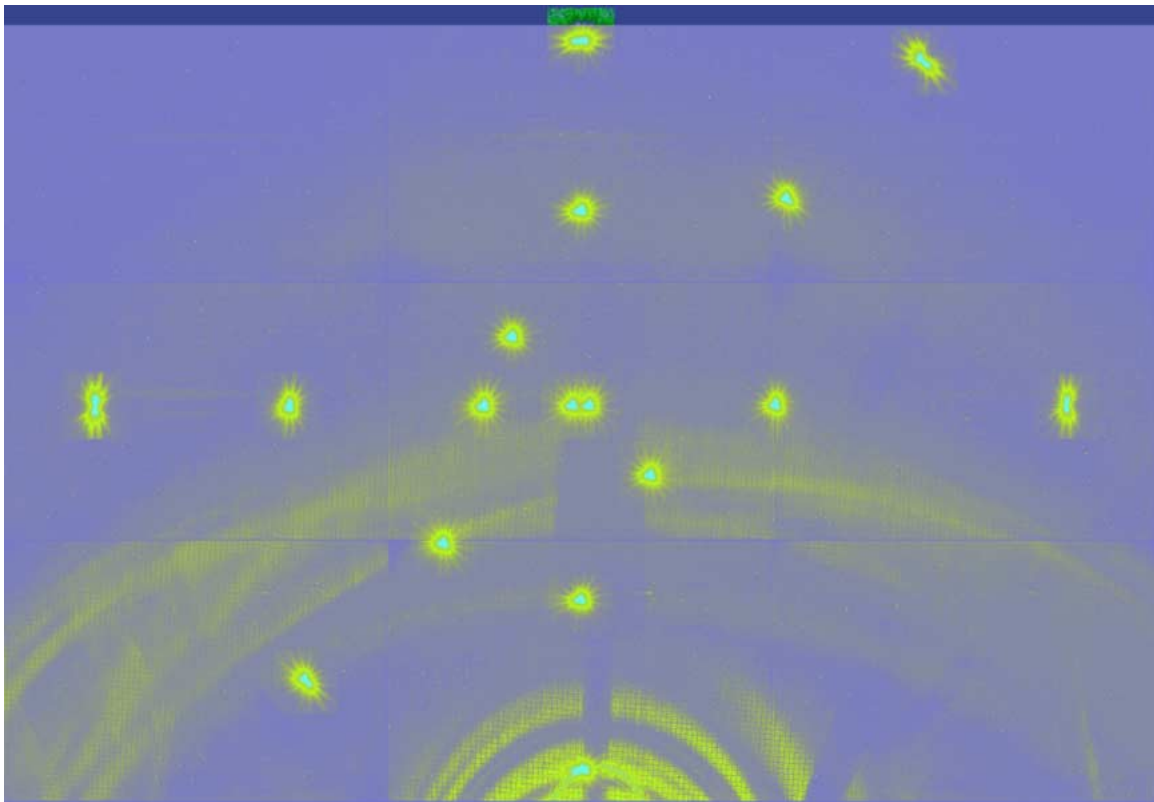


6. SIMULATION OF IMAGE THROUGH XMM OPTICS

The simulation is performed using this previous data. The straylight background is achieved by using straylight images. To simulate a wide field straylight, several straylight images taken in the 20 to 70 arcmin range are added together. The actual X-Ray radiation straylight will be more blurred due to scattering and diffuse sources and weaker due to lower reflectivity. For this example the straylight is enhanced for demonstration only.

The star field is created by using the on and off-axis images. This is a simple approach, since the image shape is energy dependent. At higher energy the contribution of the large MSs is attenuated due to lower reflectivity. However this simulated image is representative for energies up to 2 keV where the scattering impact is low, and the reflectivity fall off is not reached on the MSs.

Figure 8 : Simulated image through XMM optics



7. CONCLUSIONS

The tests performed at CSL have shown the high complexity of XMM images. Moreover due to the highly complex design of the MMs, it is very difficult to simulate XMM images in detail. These EUV on-axis and off-axis images will be used to validate the XMM numerical model¹². This model will then be used to generate in orbit calibration data file. Tests at CSL have also shown that the MM is fully qualified and that the XRB achieves the expected straylight reduction. The X ray tests have confirmed the predicted effective area within a few percents and allows to validate the numerical model¹³ in the X-Ray range. These first images of the XMM MM flight configuration give a preliminary idea of the images that will be seen through the XMM telescopes.

Acknowledgements

For almost nearly three years, five XMM MMs have been tested at CSL. It is worthful to remind that the success of all these test campaigns is mainly due to the dedication of our colleagues. Their work is greatly appreciated and is a key factor in the collection and quality of the data.

Many thanks go to ESA XMM project team for the fruitful relation and the efficient collaboration.

The vertical facility at CSL was funded by ESA XMM project under the contract number 9939/92/NL/PP.

The XMM FM MM mirrors were replicated and integrated by Media Lario (Bosisio Parini (I)) under ESA contract number 0545/93/NL/RE.

The X-ray baffles were developed by Sener (Las Arenas (S)) and Dornier under ESA contract number 11860/96/NL/RE.

The development of the RGA grating arrays is supported by NASA under contract of the University of California at Berkeley (CA. USA), with subcontracts to the Columbia University and the Lawrence Livermore National Laboratory.

References

1. Y. Stockman, J-P. Collette, J. Ph. Tock, "Optical testing of XMM flight model module I and II at the vertical EUV/X facility", SPIE 3114, pg 566, San Diego 1997.
2. Y. Stockman, I. Domken, H. Hansen, J. Ph. Tock, D. de Chambure, P. Gondoin, "XMM Flight Mirror Module environmental and optical testing", SPIE , San Diego 1998.
3. Y. Stockman, I. Domken, H. Hansen, J.Ph. Tock, T.A. Decker, A. Rasmussen, T. den Boggende, J.W. den Herder, G. Bagnasco, D. de Chambure, C. Erd, Ph. Gondoin, "XMM Flight Mirror Module with Reflection Grating Assembly and X-ray baffle testing", SPIE 3445 , San Diego 1998.
4. D. de Chambure, R. Lainé, K. van Katwijk, J. van Casteren & P. Glaude, "Producing the X-Ray Mirrors for ESA's XMM Spacecraft", ESA bulletin 89, February 1997
5. F. Jansens, "XMM observatory : a scientific and technical overview", SPIE 3444, San Diego 1998
6. A.C. Brinkman, H.J.M. Aarts, A.J.F. den Boggende, T. Bootsma, L. Dubbeldam, , J.W. den Herder , J.S. Kaastra, P.A.J. de Korte, B.J. van Leeuwen, R. Newe, E. van Zwet, S.M. Kahn, C.J. Hailey, T.A. Decker, F.B.S. Paerels, S.M. Pratuch, A. Rasmussen, G. Branduardi-Raymont, P. Guttridge, , J.V. Bixler, K. Thomsen, A. Zehnder , C. Erd, "The Reflection Grating Spectrometer on-board of XMM", SPIE Vol. 2808, 463-480, Denver 1996.
7. J. Ph. Tock, J-P. Collette, Y. Stockman, "Calibration and upgrades of the XMM vertical EUV/X test facility; FOCALX", SPIE 3114, 554, San Diego 1997
8. J. Ph. Tock, J P Collette, I Domken, Ph Kletzkine, Y Stockman, A Vignelles, " FOCAL X : A test facility for X-ray telescopes", 3rd International Symposium on Environmental Testing For Space Programmes, Noordwijk 1997
9. J. Ph. Tock, I. Domken, JP Macau, Y. Stockman, M. Thome, Ph. Kletzkine, J. Jamar, "Satus of XMM Test programme in CSL EUV and X ray test facility : FOCALX", First XMM Workshop, these proceedings, Noordwijk 98.
10. O. Citterio, P. Conconi, M. Ghigo, C. Jamar, R. Loi, F. Mazzoleni, G. Naletto, E. Pace, Y. Stockman, G. Tondello, P. Villaresi, "Vertical test facility operating at vacuum ultraviolet for testing very thin wall grazing incidence X-ray mirrors", SPIE Vol. 2279, 1994.
11. D.de Chambure, R. Lainé, K. van Katwijk, "The X-Ray Telescopes for ESA XMM Spacecraft", SPIE 3444 , San Diego 1998.
12. Ph. Gondoin, B. Aschenbach, M. Beijersbergen, R. Egger, F. Jansen, Y. Stockman, J.P. Tock, "Calibration of the first XMM Flight Mirror Module I – Image quality ", SPIE 3444 , San Diego 1998.
13. Ph. Gondoin, B. Aschenbach, M. Beijersbergen, R. Egger, F. Jansen, Y. Stockman, J.P. Tock, "Calibration of the first XMM Flight Mirror Module II – Effective area", SPIE 3444 , San Diego 1998.